

Ultraflat, Pristine, and Robust Carbon Electrode for Fast Electron-Transfer Kinetics

Amin Morteza Najarian,^{‡,§} Ran Chen,[†] Ryan J. Balla,[†] Shigeru Amemiya,^{*,†} and Richard L. McCreery^{*,‡,§}

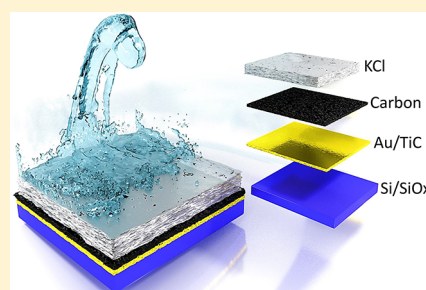
[†]Department of Chemistry, University of Pittsburgh, Pittsburgh, Pennsylvania 15260, United States

[‡]Department of Chemistry, University of Alberta, Edmonton, Alberta T6G 2R3, Canada

[§]National Institute for Nanotechnology, National Research Council Canada, Edmonton, Alberta T6G 2G2, Canada

Supporting Information

ABSTRACT: Electron-beam (e-beam) deposition of carbon on a gold substrate yields a very flat (0.43 nm of root-mean-square roughness), amorphous carbon film consisting of a mixture of sp^2 - and sp^3 -hybridized carbon with sufficient conductivity to avoid ohmic potential error. E-beam carbon (eC) has attractive properties for conventional electrochemistry, including low background current and sufficient transparency for optical spectroscopy. A layer of KCl deposited by e-beam to the eC surface without breaking vacuum protects the surface from the environment after fabrication until dissolved by an ultrapure electrolyte solution. Nanogap voltammetry using scanning electrochemical microscopy (SECM) permits measurement of heterogeneous standard electron-transfer rate constants (k^0) in a clean environment without exposure of the electrode surface to ambient air. The ultraflat eC surface permitted nanogap voltammetry with very thin electrode-to-substrate gaps, thus increasing the diffusion limit for k^0 measurement to >14 cm/s for a gap of 44 nm. Ferrocene trimethylammonium as the redox mediator exhibited a diffusion-limited k^0 for the previously KCl-protected eC surface, while k^0 was 1.45 cm/s for unprotected eC. The k^0 for $Ru(NH_3)_6^{3+/2+}$ increased from 1.7 cm/s for unprotected eC to above the measurable limit of 6.9 cm/s for a KCl-protected eC electrode.



The widespread use of carbon materials in electrochemistry has stimulated research over several decades into the factors that control carbon electrode behavior and its dependence on surface morphology, cleanliness, and preparation.^{1,2} More recent developments of graphene, carbon nanotube, and diamond electrodes for electrochemical applications has continued the intense interest in the dependence of performance on underlying carbon structure and electronic properties. Arrival at firm conclusions about kinetic effects of carbon electrode materials and preparation has been complicated by variations in carbon source and microstructure, variable cleanliness of surface preparation and electrolytes, and the electronic properties of the underlying carbon materials.^{3–6} A particular problem is the adsorption of adventitious impurities on the carbon electrode surface from air or electrolyte solution preceding electrochemical experiments. With the advent of scanning probe techniques, the diffusion limit for determining the standard heterogeneous electron-transfer (ET) rate constant (k^0) has increased substantially over that possible with cyclic voltammetry. Depending on the size of the ultramicroelectrode and the cell geometry, k^0 values exceeding 10 cm/s have been reported at metal and carbon electrodes.^{7–9} For graphene and highly ordered pyrolytic graphite (HOPG) electrodes, impurity adsorption can significantly affect the k^0 values obtained with scanning electrochemical microscopy (SECM),^{8,10–13} thus complicating interpretation of electrode effects on kinetic results. The current report was motivated both by the wide interest in

electrode kinetics at carbon electrode surfaces and difficulties obtaining and maintaining a very clean carbon surface.

Electron-beam-deposited carbon (eC) is an uncommonly studied carbon material which was examined initially for making transparent carbon electrodes,^{14,15} and later for more general electrochemistry.¹⁶ The very smooth surface of eC deposited on silicon substrates approached atomic dimensions [root-mean-square (rms) roughness <0.2 nm], and initial voltammetry at n-Si/eC electrodes showed ET rate constants from cyclic voltammetry (CV) comparable to those from glassy carbon (GC) and pyrolyzed photoresist films (PPF).¹⁶ In electrochemical applications, eC has some of the properties of boron-doped-diamond (BDD),^{2,17–19} such as significant sp^3 content, hardness, and stability, but does not have the microcrystalline structure of BDD and can be made very flat. eC also resembles electron cyclotron resonance sputtered carbon surfaces,^{20–22} and does not require custom deposition equipment. Recently, eC was used for fabrication of molecular electronic devices, in which its very flat surface (rms roughness <0.4 nm) was valuable for either or both the substrate²³ or top electrodes.²⁴ The relatively low conductivity of eC and resulting ohmic potential losses can be significant,¹⁶ but these errors become negligible when eC is

Received: September 22, 2017

Accepted: November 13, 2017

Published: November 14, 2017

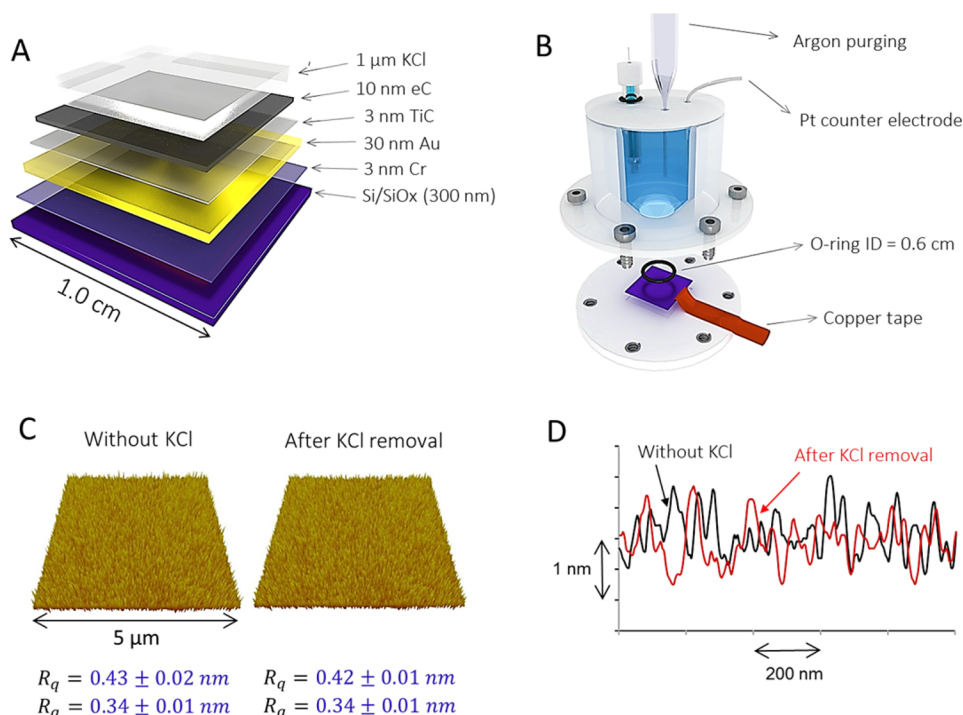


Figure 1. (A) Schematic illustration of deposited layers with indicated thicknesses on Si/SiO_x substrate. Each sample chip is 1.0 cm × 1.0 cm. (B) Schematic of “macro” electrochemical cell used for routine voltammetry. (C) AFM images from the surface of Si/SiO_x₃₀₀/Cr₃/Au₃₀/TiC₃/eC₁₀ without deposition of KCl and after removal of deposited KCl. R_a and R_q are average and root-mean-square roughness, respectively. (D) AFM line scan profiles of the surfaces shown in panel C.

deposited on a thin layer of metal, usually Au.²³ The Au/eC bilayer is sufficiently transparent for optical spectroscopy, and the flatness of the eC layer is unchanged by the underlying metal layer.²³ Molecular electronic junctions made with Au/eC bilayers for both substrate and top electrodes have demonstrated excellent stability, and their transparency permits observation of light emission from the device interior.^{25–27}

The current study of ET kinetics on eC electrodes was motivated by three aspects enabled by modern SECM techniques for monitoring electrochemical kinetics combined with the unusual properties of eC. First, the very flat eC surface permits high-performance nanogap voltammetry in ultrapure water to avoid organic contamination shown to significantly impede accurate determination of k° at carbon electrodes.^{5,6,11–13,28,29} Second, eC is amorphous, consisting of a disordered combination of ~30% sp³- and ~70% sp²-hybridized carbon;²³ hence, it is the opposite extreme of ordered carbon materials such as graphene or HOPG. Third, it is possible to electron-beam deposit a protective layer of KCl on the newly deposited Au/eC electrode without breaking vacuum. Subsequently, the KCl layer greatly reduces exposure of the eC surface to airborne impurities outside of the vacuum chamber. Once the SECM cell and equipment are assembled in a clean atmosphere, the KCl layer is dissolved in a KCl solution of a redox-active molecule prepared from ultrapure water (<1 ppb total organic carbon), thus assuring that the first exposure of the electrode outside the vacuum where it was deposited is to the electrolyte solution under study. After examining basic voltammetry and electrochemical characteristics of Au/eC electrodes, k° values for (ferrocenylmethyl)trimethylammonium (FcTMA⁺) and Ru(NH₃)₆³⁺ redox systems were examined and compared to existing methods. The properties of eC as an electrode material and its suitability for SECM kinetic measure-

ments appear promising for continued electrode kinetic investigations.

EXPERIMENTAL SECTION

Chemicals and Materials. The hexafluorophosphate salt of FcTMA⁺ was prepared by the metathesis of its iodide salt (Strem Chemicals, Newburyport, MA) and ammonium hexafluorophosphate (Strem Chemicals). KCl (≥99%, Sigma-Aldrich, St. Louis, MO) and Ru(NH₃)₆Cl₃ (99%, Strem Chemicals) were used as received. A Milli-Q Advantage A10 water purification system (EMD Millipore, Billerica, MA) was used to obtain UV-treated ultrapure water with a total organic carbon (TOC) value of 2–3 ppb as measured by using an internal online TOC monitor. The final product of the Milli-Q water purification process was passed through a specific activated-carbon filter (VOC Pak, EMD Millipore) to further reduce TOC to <1 ppb.¹¹ Filtered water was collected in a class 100 vertical laminar flow hood (AC632TLFC, AirClean Systems, Raleigh, NC) equipped with a bonded carbon filter (ACF100, AirClean Systems) to minimize airborne contamination.¹² The Milli-Q system was fed with the water (15.0 MΩ·cm) purified from tap water by using Elix 3 Advantage (EMD Millipore).

Fabrication and Atomic Force Microscopy Characterization of eC Electrodes. Layers of materials shown in Figure 1A were deposited in an electron beam chamber at below 6×10^{-6} Torr as detailed in the Supporting Information to obtain eC electrodes, which were characterized by atomic force microscopy (AFM), scanning electron microscopy (SEM), X-ray photoelectron spectroscopy (XPS), ultraviolet photoelectron spectroscopy (UPS), and Auger spectroscopy. A 3 nm thick titanium carbide layer was added to the previous procedure²³ between Au and eC to prevent occasional delamination of eC from the Au surface during electrochemical experiments. Previous experi-

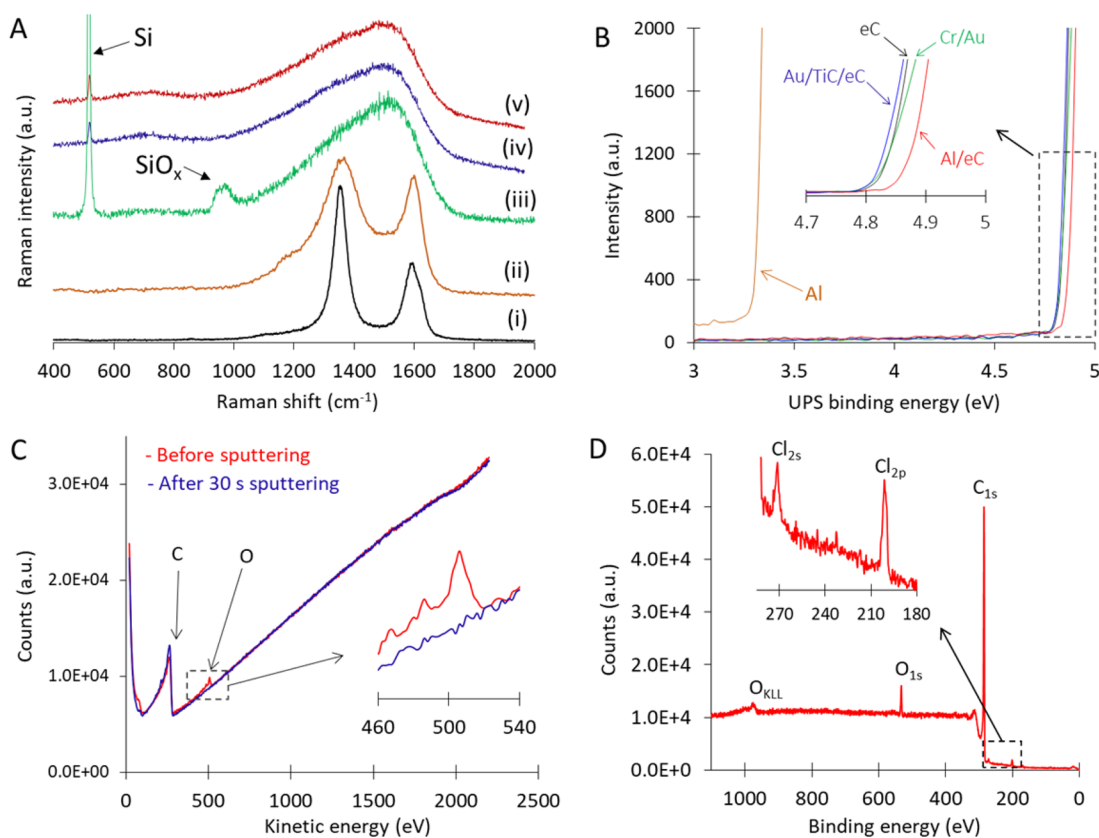


Figure 2. (A) Raman spectra of (i) GC, (ii) Si/SiO_x/PPF, (iii) Si/SiO_x/eC, (iv) Si/SiO_x/Cr/Au/TiC/eC/KCl, and (v) Si/SiO_x/Cr/Au/TiC/eC after removal of deposited KCl layer. (B) UPS spectra of eC, Al, Al/eC, Cr/Au, and Au/TiC/eC surfaces. The substrate for all cases was Si/SiO_x. (C) Auger electron spectra of Si/SiO_x/Cr₃/Au₃₀/TiC₃/eC₁₀ before and after 30 s of sputtering. The inset is the magnification of the oxygen peak at 505 eV. (D) XPS survey spectrum of a Si/SiO_x/Cr₃/Au₂₀/TiC₅/eC₁₀ surface after removal of a 1 μm thick KCl layer. Inset is a magnification of the peaks related to chlorine.

ence²⁴ indicates that eC thicknesses of 2–30 nm result in negligible ohmic errors in molecular junctions, and the eC layer was 10 nm thick in the current work. KCl was e-beam-deposited on the eC surface without breaking vacuum, using a compressed pellet of KCl instead of graphite rods as the deposition target. While other materials may be used for protection of the eC surface, KCl is common in electrochemistry and suitable for aqueous solutions. Figure 1C compares AFM images for a Si/SiO_x₃₀₀/Cr₃/Au₃₀/TiC₃/eC₁₀ surface without the KCl protective layer and from a Si/SiO_x₃₀₀/Cr₃/Au₃₀/TiC₃/eC₁₀/KCl₁₀₀₀ sample after the KCl layer was removed with a water rinse. Subscripts on each layer indicate thicknesses in nanometers and were kept constant throughout the study. Standard deviations in rms and average roughness (R_q and R_a , respectively) are based on four different 5 μm × 5 μm areas on each sample. The comparison clearly shows that the KCl deposition has no observable effect on the eC surface roughness and that a water rinse rapidly removes the salt from the surface with no visible residue. This conclusion is also supported by comparison of AFM line scans of the fabricated electrodes with and without KCl treatment indicated in Figure 1D. Both uncoated and KCl-coated eC samples were exposed to air during shipment from Edmonton to Pittsburgh, but the KCl coating remained intact until the sample was exposed to the electrolyte solution in the SECM apparatus. Figure 1B is a schematic of the electrochemical cell used for conventional voltammetry on Au/eC electrodes in Edmonton. SEM images of Au and Au/eC are shown in Supporting Information Figure S1.

SECM Measurements. A home-built SECM instrument with an isothermal chamber³⁰ was used as reported elsewhere.¹¹ Glass-sealed Pt tips with inner and outer diameters of ~1 and ~2 μm were fabricated by laser-assisted pulling, heat annealing, and focused-ion-beam milling.^{31,32} A Pt tip was cleaned in piranha solution (a 1:3 mixture of 30% H₂O₂ and 95.0–98.0% H₂SO₄) and in ultrapure water immediately before the tip was immersed in the electrolyte solution in the sealed SECM cell¹¹ with an eC electrode. *Caution: piranha solution reacts violently with organics and should be handled with extreme care!* The glass and Teflon components of the cell were also cleaned in piranha solution and in ultrapure water. The tip was protected from electrostatic discharge^{12,28} under sufficiently high humidity (>30%).^{33–35} Pt and Ag (or Ag/AgCl) wires were used as counter and reference electrodes, respectively. SECM measurements were carried out by using a bipotentiostat (CHI 802D, CH Instruments, Austin, TX), which was modified to eliminate possible causes of tip damage.^{12,35,36}

RESULTS AND DISCUSSION

The results of spectroscopic characterization of Cr/Au/TiC/eC surfaces by Raman, Auger, UPS, and XPS are presented in Figure 2. The broad Raman band at 1200–1600 cm⁻¹ for eC on Si/SiO_x is similar to that observed for eC on Si,¹⁶ with Raman features of Si and SiO_x apparent through the partially transparent eC layer. The featureless 1200–1600 cm⁻¹ band of eC on both SiO_x and Au/TiC indicates significantly more disorder than in either GC or PPF, and the presence of both sp²- and sp³-hybridized carbon.

Table 1. Atomic Ratios from XPS

sample	KCl protection ^a	atom % O/C	% Ti/C	% Au/C	% Cl/C
SiOx/eC	none	3.5	ND ^b	<0.02	ND
Si/SiOx/Cr/Au/TiC/eC	none	3.5	ND	<0.02	ND
Si/SiOx/Cr/Au/TiC/eC/KCl	KCl removed <10 min before XPS	3.2	ND	<0.02	<0.8
Si/SiOx/Cr/Au/TiC/eC/KCl	KCl removed 3 weeks before XPS	7.2	ND	<0.02	<0.8
Si/SiOx/Cr/Au/TiC/eC/KCl	KCl removed after 3 weeks in air	5.1	ND	<0.02	<0.8

^aAll samples were exposed to air for <10 min before entering pump-down for XPS. ^bBelow the XPS detection limit.

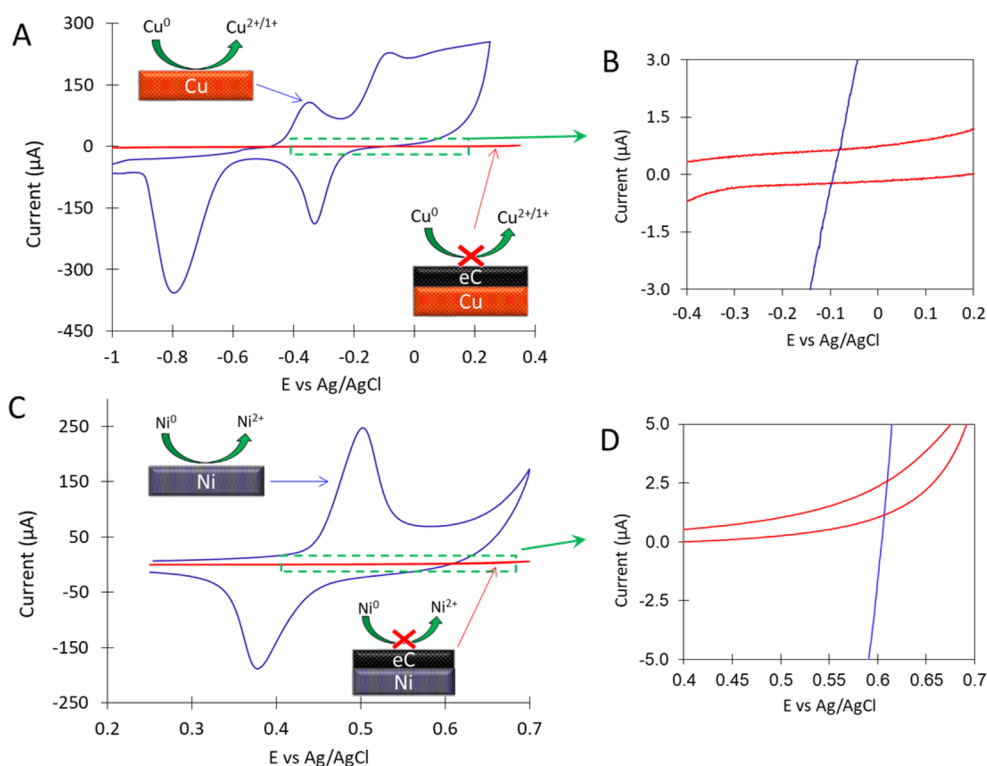


Figure 3. (A) CV for the Si/SiOx/Cr₃/Cu₄₀ and Si/SiOx/Cr₃/Cu₄₀/TiC₃/eC₁₀ surfaces in alkaline solution (NaOH 0.1 M) at 0.1 V/s. (B) Magnification of voltammograms shown in panel A for the region of Cu oxidation. (C) CV obtained for Si/SiOx/Cr₃/Ni₃₀ and Si/SiOx/Cr₃/Ni₃₀/TiC₃/eC₁₀ in alkaline solution (NaOH 0.1 M) at 0.1 V/s. (D) Magnification of voltammograms shown in panel C for the region of Ni oxidation. The area of the exposed electrode was 0.28 cm² for all cases.

Analysis of the Raman spectra combined with deconvolution of the high-resolution C_{1s} feature from XPS presented previously²³ indicates that the sp³ content of eC is ~30%, with the remainder sp²-hybridized. Pyrolysis of eC at 1000 °C substantially increased order based on the Raman spectra¹⁶ and significantly reduced the sp³ content to ~0% by Raman and ~11% by XPS.²³ The Au/TiC layer between SiOx and eC greatly reduced the Si and SiOx Raman features, as expected, but also yields a weak TiC feature in the region 600–800 cm⁻¹. These results indicate that the eC layer on Cr/Au/TiC is structurally similar to that on Si, SiOx, or SiOx/Au, while maintaining an rms roughness of ~0.4 nm. Figure 2B shows UPS spectra of eC₁₀ alone, Cr₃/Au₃₀, and Cr₃/Au₃₀/TiC₃/eC₁₀ (all on Si/SiOx), from which the onset of photoemission at ~4.8 eV indicates the work function (WF) of the surface. The onset binding energies are within experimental error (±0.1 eV) for these three surfaces, indicating that the WF of the top eC₁₀ layer is not significantly altered by the underlying metal or TiC layer. In addition, aluminum was examined due to its much lower WF compared to Au or eC. Bare Al exhibits a WF of 3.3 eV by UPS, while the Al₄₀/eC₁₀ surface is very similar to the other eC-terminated surfaces, at ~4.8 eV. The absence of observable photoemission at 3.3 eV for Al/eC is also an

indication that negligible bare Al remains on the Al/eC surface, and therefore that eC coverage of the underlying surface is complete by this measure. An Auger electron spectrum for the Cr₃/Au₃₀/TiC₃/eC₁₀ surface is shown in Figure 2C, with the peak at 250–300 eV feature corresponding to carbon and the ~500 eV peak to surface oxygen. The removal of the ~500 eV band by Ar⁺ sputtering indicates that the oxygen content is superficial and not detectable below the eC surface. Figure S2 shows Auger emission maps for the initial Cr₃/Au₃₀/TiC₃/eC₁₀ surface, showing an even distribution of both carbon and oxygen across the electrode surface. Neither Au nor Ti was detectable in the Auger survey scans (Figure 2C) or with elemental mapping (Figure S2), consistent with the absence of pinholes in the eC film detectable by Auger spectroscopy. Furthermore, deposition and removal of an ~1 μm film of KCl on the Au₂₀/TiC₃/eC₁₀ surface has no observable effect on surface roughness (Figure 1, parts C and D), or the Raman spectra.

XPS spectra of the Cr₃/Au₂₀/TiC₃/eC₁₀ surface after removal of KCl with a water rinse are shown in Figure 2D. The prominent C_{1s} and O_{1s} features are present on eC before and after KCl removal, although KCl treatment does result in residual Cl_{1s} and Cl_{2p} features, apparent in the magnified inset. Potassium and Ti

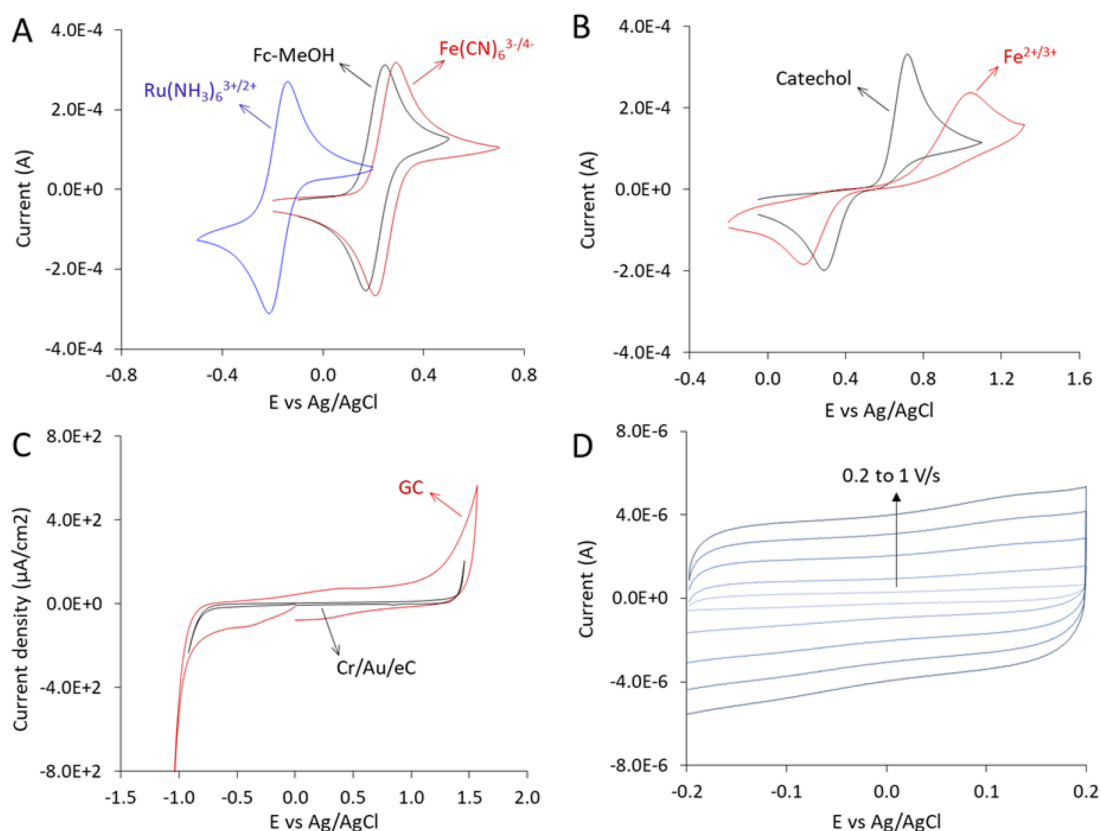


Figure 4. (A) Voltammetry on Si/SiO_x/Cr₃/Au₂₀/TiC₃/eC₁₀ as working electrode in the cell shown in Figure 1B for (A) Fe(CN)₆^{3-/4-}, Ru(NH₃)₆^{3+/2+}, and FcMeOH in 0.5 M KCl and (B) catechol and Fe^{2+/3+} in 0.1 M HClO₄. The solutions contained 2.0 mM of redox system, and the scan rate was 0.1 V/s for all cases. (C) Background current for voltammetry (0.1 V/s) in 0.1 M HClO₄ for GC and eC electrodes. The currents are normalized to the electrode area. (D) Scan rate dependent background current for the eC electrode.

features were undetectable in either survey or high-resolution XPS spectra, and the O/C ratio depends on both deposition parameters and exposure to air. Table 1 lists atomic ratios for several samples prepared with a backpressure during metal and eC layers of $<1 \times 10^{-7}$ Torr. Following brief exposure to air during sample transfer, Au/TiC/eC surfaces exhibit O/C of 3.2–3.5% both before and after KCl removal. Trace Au was detected in high-resolution scans ($<0.02\%$ Au/C), but this Au is unlikely due to the underlying Au layer, since it is also present when only eC is vapor-deposited. It is likely due to contamination from the vacuum chamber and detectable due to the high XPS sensitivity for Au element. Upon exposure of unprotected eC to air, the O/C ratio increased to 7.2% after 3 weeks, which is similar to other carbon surfaces which started with low O/C ratio.³⁷ This increase is slowed but not eliminated by KCl protection, resulting in 5.1% O/C ratio after 3 weeks in air preceding KCl removal and immediate transfer to the XPS vacuum. Figure S3 shows the effect of Ar⁺ sputtering on the eC surface, using an Ar⁺ flux which would remove SiO_x at a rate of 2 nm/min. The C_{1s} XPS peak remained unchanged by prolonged sputtering for >140 min and the O_{1s} peak decreased rapidly, indicating that the oxygen is superficial. In summary, the XPS results indicate complete coverage of TiC with eC and that KCl treatment results in a low residue of Cl atoms (<0.8 atom %), presumably due to reactions of surface radicals with chloride ion. Additional XPS spectra of eC before and after KCl treatment are shown in Figures S4 and S5.

Although the absence of Au or Ti responses in the Auger and XPS spectra implies good surface coverage with low pinhole

density, the possibility of exposure of the metal underlying eC was examined further. Coverage of graphene on metal electrodes has been assessed by attempting to oxidize Cu or Ni electrodes underneath single or multilayer graphene.^{5,38–40} Figure 3A (blue curve) shows voltammetry of an unmodified Cu electrode in 0.1 M NaOH electrolyte, exhibiting prominent features characteristic of Cu corrosion and redeposition. A Cu electrode with 10 nm of eC (i.e., Si/SiO_x/Cr₄/Cu₄₀/eC₁₀) in the same electrolyte yielded the red voltammogram in Figure 3A, with the dotted region expanded in Figure 3B. No features for Cu redox activity are evident with the eC-modified electrode, and the current for the first oxidation peak at $E = -0.33$ V is a factor of >2000 smaller than that on the bare Cu electrode. The blockage of metal oxidation by eC₁₀ is similar for a Ni electrode, shown in Figure 3, parts C and D, with no observable redox features apparent for the Ni/eC₁₀ electrode in 0.1 M NaOH. Application of an $\sim 1 \mu\text{m}$ thick layer of KCl on Cu/eC in vacuum followed by KCl dissolution had no observable effect on blocking the Cu oxidation waves, indicating no apparent damage to the eC layer from KCl.

To provide an initial assessment of electrochemical kinetics of Au/TiC/eC electrodes, slow scan (0.1 V/s) CVs for five commonly studied aqueous redox systems are shown in Figure 4, all using the cell shown in Figure 1B and the as-deposited Au/TiC/eC surfaces. FcMeOH⁺⁰, Fe(CN)₆^{3-/4-}, and Ru(NH₃)₆^{3+/2+} exhibit reversible ET for the slow scans employed, while Fe^{3+/2+} and catechol exhibit the significantly larger peak separations characteristic of slow ET. The latter two systems have been shown to require adsorption sites (catechol) or surface

C=O groups ($\text{Fe}^{3+/2+}$) for electrocatalysis on GC electrodes, with their kinetics strongly dependent on surface history and cleanliness on glassy carbon electrodes.^{41–44} Adsorption of anthraquinone on eC is much weaker than on GC,¹⁶ consistent with weak catechol electrocatalysis.⁴¹ Figure 4C shows voltammetric scans in 0.1 M HClO_4 electrolyte for Au/TiC/eC and GC electrodes, normalized for electrode area. Although the two materials have similar potential limits, they differ significantly in capacitance and electrode redox reactions, with the redox wave for surface quinones (~ 0.2 V) absent on eC. Faster scan rate voltammograms of eC at low potentials (Figure 4D) show classical capacitance behavior, with nearly undetectable surface redox reactions. The capacitance was assessed quantitatively by ac impedance spectroscopy using the common RC model for an electrochemical cell shown in the Supporting Information (Figures S6–S8), with the results listed in Table 2.

Table 2. Capacitance of Carbon Electrodes in 0.1 M HClO_4

	polishing	capacitance ($\mu\text{F}/\text{cm}^2$) ^a	no. of samples	RSD, %
Au/TiC/eC	none	9.5	3 ^b	2.0
Au/TiC/eC	none	9.6	9 ^c	9.5
GC	alumina 0.05 $\mu\text{m}/\text{H}_2\text{O}$	27.1	3	22.8
GC	alumina 0.3 $\mu\text{m}/\text{H}_2\text{O}$	58.6	3	12.8
GC	alumina 1 $\mu\text{m}/\text{H}_2\text{O}$	84.3	3	13.6
GC	Buehler SiC grinding paper P2400	346	3	3.0
GC	Buehler SiC P1200	834	3	1.5

^aFrom ac impedance with $E = 0.0$ V vs Ag/AgCl, amplitude = 50 mV.

^bElectrodes from one Au/TiC/eC deposition. ^cElectrodes from three different depositions.

The capacitance of the Au/TiC/eC electrode was 9.6 ± 0.92 $\mu\text{F}/\text{cm}^2$, compared to 27–84 $\mu\text{F}/\text{cm}^2$ for GC following the common procedure of polishing in an Al_2O_3 slurry with water. In addition, the reproducibility of the low eC capacitance was better (relative standard deviation of 2% in one batch, 9.5% across three batches) than that from polishing (13–22%). At least some of the decreased capacitance for eC compared to GC is due to reduced microscopic surface area, but the sp^3 content, low O/C ratio, and smaller or absent surface redox reactions are likely contributing factors.

The high electrochemical reactivity of eC surfaces was further assessed by employing nanogap voltammetry based on SECM.³¹ This technique has been used to address high k° values of up to 25 cm/s at various carbon materials in solution, i.e., HOPG,^{11,12} graphene,¹⁰ GC,⁴⁵ and BDD,⁴⁵ in contrast to scanning electrochemical cell microscopy, which measures k° values of 0.1–1.0 cm/s at bare surfaces of macroscopic substrates exposed to ambient air.^{46,47} In the current study, all experimental nanogap voltammograms fit well to theoretical voltammograms³¹ (see the Supporting Information) without considering a heterogeneous self-exchange reaction at the glass sheath of a Pt ultramicroelectrode tip⁴⁸ or a double layer effect from the glass surface charge.⁴⁹ This double layer effect was simulated recently by Unwin and co-workers,⁵⁰ but was not needed to fit their reported nanogap voltammograms.⁴⁵

Using the SECM apparatus shown schematically in Figure 5, we were able to form a nanometer-wide gap between the flat eC surface and a Pt ultramicroelectrode tip to achieve the high mass-transport conditions across the gap required for nanogap voltammetry of fast ET reactions. Specifically, a tip was

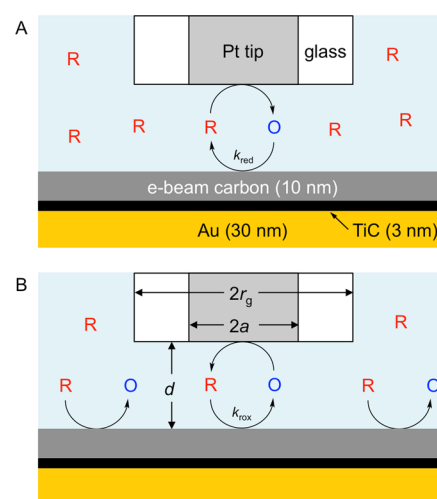


Figure 5. Scheme of (A) feedback and (B) SG/TC modes of SECM at an eC electrode. Heterogeneous reduction and oxidation rate constants are represented by k_{red} and k_{ox} , respectively.

positioned at a nanometer distance from the eC surface by monitoring approach curves based on the positive feedback mode of SECM (Figure 5A), where the tip potential, E_T , was set to electrolyze a redox mediator in solution (e.g., $\text{R} = \text{FcTMA}^+$) at a diffusion-limited rate. When the tip was far away from the substrate surface, a steady-state diffusion-limited tip current, $i_{T,\infty}$, was obtained as given by

$$i_{T,\infty} = 4xnFDc_0a \quad (1)$$

where x is a function of RG ($= r_g/a$; a and r_g are the tip radii of Pt and glass sheath as indicated in Figure 5B),⁵¹ n is the number of electrons transferred in the tip reaction ($= 1$ in this study), and D and c_0 are the diffusion coefficient and concentration of the original redox mediator. The tip current was enhanced as the tip approached within a short distance (typically the tip diameter) from an eC surface, where the substrate potential, E_S , was set to electrolyze the tip-generated species (e.g., $\text{O} = \text{FcTMA}^{2+}$ in Figure 5A) at a diffusion-limited rate. Very similar SECM approach curves were obtained at eC surfaces prepared with (Figure S9A) and without (Figure S9B) a KCl layer by employing sharp ~ 1 μm diameter Pt tips with small RG of ~ 2 . The tip current based on the oxidation of FcTMA^+ was enhanced by a factor of up to 10 with respect to $i_{T,\infty}$ at both substrates before the tip contacted the substrate. Experimental approach curves at both substrates fitted very well with theoretical curves based on the diffusion-limited positive feedback effect⁵¹ until a tip–substrate distance, d , decreased to ~ 45 nm. This distance was extremely short with respect to the tip radius, i.e., d/a of ~ 0.09 , and was as short as that achieved with an atomically flat surface of HOPG.¹¹ These results as well as AFM images (Figure 1C) ensured the similarly excellent flatness of eC surfaces exposed by dissolving a KCl layer or prepared without a KCl layer.

The electrochemical reactivity of eC surfaces for the $\text{FcTMA}^{2+/+}$ couple was studied by nanogap voltammetry based on the feedback mode as well as the substrate generation/tip collection (SG/TC) mode (Figure 5B). Experimentally, a pair of nanogap voltammograms was obtained by monitoring the tip current in feedback and SG/TC modes while the tip position was fixed during cycles of substrate potential (Figure 6). A family of paired nanogap voltammograms was obtained by systematically

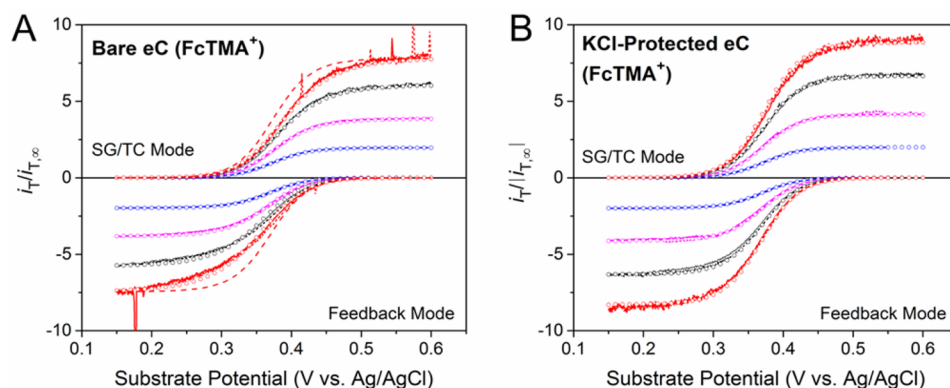


Figure 6. Nanogap voltammograms of 0.3 mM FcTMA⁺ in 1 M KCl at eC electrodes prepared without (A) and with (B) a protective KCl layer obtained using 1.01 and 1.04 μm diameter Pt tips (RG = 2.0), respectively. Forward and reverse waves are represented by solid and dotted lines, respectively. $E_T = 0.55$ and 0.15 V vs Ag/AgCl in feedback and SG/TC modes, respectively. Potential sweep rate, 0.05 V/s. Circles represent theoretical curves with $E^{\circ'} = 0.371$ V vs Ag/AgCl as well as parameters listed in Table S1 including gap widths of 44–275 nm. Dashed lines in panel A represent theoretical reversible curves with $\lambda = 10$ at the shortest tip–substrate distance of 49 nm.

decreasing the tip–substrate distance, which enhanced the tip current owing to a higher mass-transport condition across a narrower gap (the same color is used for a pair of voltammograms measured at the same tip position in Figure 6). When bare eC electrodes prepared without a KCl layer were studied (Figure 6A), nanogap voltammograms were broader than reversible ones and fitted well with kinetically limited voltammograms calculated using eqs S1 and S5 with various tip–substrate distances of 49–262 nm, yielding consistent k° values of 1.45 ± 0.06 cm/s (details in Table S1) and an α value of 0.5. These k° values were too high to be measured by conventional CV based on plots of the substrate current against the substrate potential, where k° values of up to 0.95 cm/s are measurable even at a potential sweep rate, ν , of 10 V/s, i.e., $k^{\circ} \geq 0.3\nu^{1/2}$.⁵² However, this k° is much lower than that reported for HOPG in ultraclean electrolyte (>12 cm/s) and comparable to the 0.7–1.7 cm/s at contaminated HOPG surfaces as measured by SECM-based nanogap voltammetry.¹¹ This result implies that nonprotected eC surfaces were adsorbing airborne contaminants between the vacuum used for fabrication and the electrochemical cell.

The application of an ~ 1 μm thick KCl layer in vacuum immediately after deposition of eC should greatly reduce airborne contamination, since the eC surface is exposed only to ultrapure electrolyte when the KCl is dissolved in the SECM cell. Figure 6B shows paired nanogap voltammograms at eC surfaces protected by KCl between deposition and SECM, showing excellent fits with reversible voltammograms calculated with $\lambda = k^{\circ}d/D = 10$ in eqs S1 and S5 with various tip–substrate distances of 44–275 nm. Consistent k° and d values were obtained from feedback and SG/TC branches of each nanogap voltammogram (Table S1). Such ideal nanogap voltammograms without an effect of contamination have been difficult to obtain and have been reported previously only with relatively clean HOPG surfaces covered with a nanometer-thick protective layer of condensed water.¹² The reversible nanogap voltammograms indicate negligible ohmic potential drop across the thin Au-supported eC film with high conductivity²³ despite the high current density at the eC surface under the 1 μm diameter Pt tip. A diffusion-limited λ value of 10 yields an extremely high k° value of 14 cm/s with $D = 6.0 \times 10^{-6}$ cm²/s and $d = 44$ nm. This k° value is a diffusion-limited minimum value, i.e., the actual k° value is higher than 14 cm/s, and is similar to the corresponding k° value of ≥ 12 cm/s for the FcTMA^{2+/+} couple at water-protected

HOPG surfaces.¹² The minimum k° value of KCl-protected eC surfaces is 10 times higher than the k° value of bare eC surfaces. High k° values at clean eC surfaces were addressable owing to high mass-transport conditions across the narrow tip–substrate gap enabled by the very flat eC surface. In contrast, conventional CVs for the KCl-protected Au/eC surface were reversible even at 10 V/s to yield a diffusion-limited minimum k° value of 0.95 cm/s from a criteria of $k^{\circ} \geq 0.3\nu^{1/2}$ or 0.2 cm/s from a fit with a simulated CV (Figure S10B).

It should be noted that the diffusion-limited minimum k° values of 14 cm/s at clean eC surfaces are still much lower than the highest k° value expected for the outer-sphere mechanism in the adiabatic regime⁵³ (Table 3). A k° value for a heterogeneous

Table 3. Theoretical and Experimental k° Values for FcTMA^{2+/+} and Ru(NH₃)₆^{3+/2+} Couples

redox couple	k° (cm/s)	
FcTMA ^{2+/+}	100 ^a	Marcus theory
	1.45 ± 0.06 ^b	nonprotected eC
	≥ 14 ^b	KCl-protected eC
Ru(NH ₃) ₆ ^{3+/2+}	≥ 12 ^c	water-protected HOPG
	2.0 ^a to 2.5 ^d	Marcus theory
	1.7 ± 0.2 ^e	nonprotected eC
	≥ 6.9 ^b	KCl-protected eC

^aFrom eq 2. ^bThis work. ^cFrom ref 12. ^dFrom ref 55. ^eThis work, with Au/eC electrode instead of Au/TiC/eC.

adiabatic outer-sphere reaction of a redox couple is related to its homogeneous self-exchange rate constant, k_{ex} , by Marcus theory⁵³ as

$$k^{\circ} = Z_{\text{het}} \sqrt{\frac{k_{\text{ex}}}{Z_{\text{bi}}}} \quad (2)$$

where $Z_{\text{het}} \sim 10^4$ cm/s and $Z_{\text{bi}} \sim 10^{11}$ M⁻¹ s⁻¹ are heterogeneous and bimolecular collision frequencies, respectively. A k° value of 1×10^2 cm/s is obtained from eq 2 with a k_{ex} value of 9×10^6 M⁻¹ s⁻¹ for the FcTMA^{2+/+} couple in water.⁵⁴ The outer-sphere mechanism of this redox couple at clean eC surfaces is supported by CV as discussed in the Supporting Information.

Nanogap voltammetry of the Ru(NH₃)₆^{3+/2+} couple at eC surfaces without KCl protection is shown in Figure S11A for both SG/TC and feedback modes and indicates a k° of 1.7 ± 0.2 cm/s

(Table S2). With KCl protection followed by removal directly in the electrolyte, the voltammetry shows excellent agreement with a diffusion-controlled rate with $k^\circ \geq 6.9$ cm/s (Figure S11B). Both branches of nanogap voltammograms of $\text{Ru}(\text{NH}_3)_6^{3+}$ at clean eC surfaces were fitted well with reversible voltammograms calculated with $\lambda = 10$ (circles) and consistent d values in eqs S6 and S7. This ideal voltammetric behavior indicates negligible contamination of the eC surface. The λ value corresponds to $k^\circ = 6.9$ cm/s at the shortest tip–substrate distance of 97 nm (Table S2). Conventional CV at 10 V/s showed the expected reversible behavior (Figure S12). The reported adiabatic limit for $\text{Ru}(\text{NH}_3)_6^{3+/2+}$ is $k^\circ = 2.5$ cm/s⁵⁵ and is 2.0 cm/s expected from eq 2 for $\text{Ru}(\text{NH}_3)_6^{3+/2+}$ with a k_{ex} value of $4 \times 10^3 \text{ M}^{-1} \text{ s}^{-1}$.⁵⁶ As shown in Figure S11B, the voltammograms in feedback mode differ significantly from calculated for $k^\circ = 2.5$ cm/s, indicating a significantly faster k° than the adiabatic outer-sphere limit (Table 3). Interestingly, k° values larger than adiabatic limits were also determined previously for the presumably outer-sphere $\text{Ru}(\text{NH}_3)_6^{3+/2+}$ couple at other electrode materials by using nanoelectrochemical approaches, i.e., $k^\circ = 79$ ⁵⁷ and 17.0⁷ cm/s at Pt nanoelectrodes, 13.5 cm/s at Au nanoelectrodes,⁵⁸ ≥ 10 cm/s at chemical vapor deposition (CVD)-grown carbon nanoelectrodes,⁸ 10 cm/s at individual single-walled carbon nanotubes,⁵⁹ and 36 cm/s at single Pt nanoparticles.³⁵ We hypothesize that the heterogeneous ET reaction of the $\text{Ru}(\text{NH}_3)_6^{3+/2+}$ couple is not only mediated through the outer-sphere pathway, but also through the inner-sphere pathway, to yield an overall ET rate that is the sum of an outer-sphere ET rate and an inner-sphere ET rate. Accordingly, the corresponding overall k° value is higher than expected for the adiabatic outer-sphere mechanism from the Marcus theory. This hypothesis will be addressed in our future work by quantitatively treating the ET kinetics based on both outer-sphere and inner-sphere pathways.

CONCLUSION

E-beam-deposited carbon on a Au/TiC substrate provides a very flat electrode surface which permits SECM nanogap voltammetry and determination of k° values exceeding 14 cm/s. Although the eC surface has a roughness close to that of atomically flat HOPG basal plane, it is structurally very disordered, consisting of an amorphous carbon matrix with an approximately 70/30 mixture of sp^2 - and sp^3 -hybridized carbon. Protection by KCl deposited after eC formation in the same vacuum protects the eC surface from airborne contamination and results in ideal SECM voltammetry in both feedback and SG/TC modes. With such protection, the k° values for both FcTMA^+ and $\text{Ru}(\text{NH}_3)_6^{3+/2+}$ exceed the fastest values possible with the current SECM measurements. The k° for $\text{Ru}(\text{NH}_3)_6^{3+/2+}$ on eC is comparable to that determined on Pt, Au, nanotube, and HOPG, and the fact that it exceeds predictions from Marcus theory is a subject of further study. In particular, decreasing the microelectrode diameter and, subsequently, narrowing a tip–substrate gap should further increase accessible k° values, and KCl coatings should mitigate concerns about surface contamination. Combined with the use of ultrapure electrolytes,^{12,13} KCl protection may be applied to other vacuum-deposited electrode materials to permit electrode kinetics studies with minimal surface contamination.

ASSOCIATED CONTENT

Supporting Information

The Supporting Information is available free of charge on the ACS Publications website at DOI: 10.1021/acs.analchem.7b03903.

Additional characterization and electrochemical analysis (PDF)

AUTHOR INFORMATION

Corresponding Authors

*E-mail: amemiya@pitt.edu.

*E-mail: mcreery@ualberta.ca.

ORCID

Amin Morteza Najarian: 0000-0002-0455-0451

Ran Chen: 0000-0002-6808-4381

Ryan J. Balla: 0000-0003-2374-9535

Shigeru Amemiya: 0000-0001-7357-4505

Richard L. McCreery: 0000-0002-1320-4331

Notes

The authors declare no competing financial interest.

ACKNOWLEDGMENTS

This work was supported by the University of Alberta, the National Research Council of Canada, the Natural Sciences and Engineering Research Council of Canada, and Alberta Innovates. S.A. expresses thanks for support by the National Science Foundation (CHE 1608703). R.J.B. was supported by a Dietrich School of Arts and Sciences Graduate Fellowship from the University of Pittsburgh.

REFERENCES

- (1) McCreery, R. L. *Chem. Rev.* **2008**, *108*, 2646–2687.
- (2) Swain, G. M. In *Electroanalytical Chemistry*; Bard, A. J., Rubinstein, I., Eds.; Dekker: New York, 2004; pp 181–277.
- (3) McCreery, R. L.; McDermott, M. T. *Anal. Chem.* **2012**, *84*, 2602–2605.
- (4) Amemiya, S.; Chen, R.; Nioradze, N.; Kim, J. *Acc. Chem. Res.* **2016**, *49*, 2007–2014.
- (5) Velický, M.; Bradley, D. F.; Cooper, A. J.; Hill, E. W.; Kinloch, I. A.; Mishchenko, A.; Novoselov, K. S.; Patten, H. V.; Toth, P. S.; Valota, A. T.; Worrall, S. D.; Dryfe, R. A. W. *ACS Nano* **2014**, *8*, 10089–10100.
- (6) Zou, Y.; Walton, A. S.; Kinloch, I. A.; Dryfe, R. A. W. *Langmuir* **2016**, *32*, 11448–11455.
- (7) Sun, P.; Mirkin, M. V. *Anal. Chem.* **2006**, *78*, 6526–6534.
- (8) Chen, R.; Hu, K.; Yu, Y.; Mirkin, M. V.; Amemiya, S. *J. Electrochem. Soc.* **2016**, *163*, H3032–H3037.
- (9) Guell, A. G.; Ebejer, N.; Snowden, M. E.; McKelvey, K.; Macpherson, J. V.; Unwin, P. R. *Proc. Natl. Acad. Sci. U. S. A.* **2012**, *109*, 11487–11492.
- (10) Chen, R.; Nioradze, N.; Santhosh, P.; Li, Z.; Surwade, S. P.; Shenoy, G. J.; Parobek, D. G.; Kim, M. A.; Liu, H.; Amemiya, S. *Angew. Chem., Int. Ed.* **2015**, *54*, 15134–15137.
- (11) Nioradze, N.; Chen, R.; Kurapati, N.; Khvataeva-Domanov, A.; Mabic, S.; Amemiya, S. *Anal. Chem.* **2015**, *87*, 4836–4843.
- (12) Chen, R.; Balla, R. J.; Li, Z.; Liu, H.; Amemiya, S. *Anal. Chem.* **2016**, *88*, 8323–8331.
- (13) Li, Z.; Kozbial, A.; Nioradze, N.; Parobek, D.; Shenoy, G. J.; Salim, M.; Amemiya, S.; Li, L.; Liu, H. *ACS Nano* **2016**, *10*, 349–359.
- (14) Mattson, J. S.; Smith, C. A. *Anal. Chem.* **1975**, *47*, 1122–1125.
- (15) DeAngelis, T. P.; Hurst, R. W.; Yacynych, A. M.; Mark, H. B., Jr.; Heineman, W. R.; Mattson, J. S. *Anal. Chem.* **1977**, *49*, 1395–1398.
- (16) Blackstock, J. J.; Rostami, A. A.; Nowak, A. M.; McCreery, R. L.; Freeman, M.; McDermott, M. T. *Anal. Chem.* **2004**, *76*, 2544–2552.

- (17) Jarošová, R.; De Sousa Bezerra, P. M.; Munson, C.; Swain, G. M. *Phys. Status Solidi A* **2016**, *213*, 2087–2098.
- (18) Kim, D. Y.; Merzougui, B.; Swain, G. M. *Chem. Mater.* **2009**, *21*, 2705–2713.
- (19) Wang, S.; Swain, G. M. *J. Phys. Chem. C* **2007**, *111*, 3986–3995.
- (20) Kamata, T.; Kato, D.; Ida, H.; Niwa, O. *Diamond Relat. Mater.* **2014**, *49*, 25–32.
- (21) Kato, D.; Niwa, O. *Anal. Sci.* **2013**, *29*, 385–392.
- (22) Niwa, O.; Jia, J.; Sato, Y.; Kato, D.; Kurita, R.; Maruyama, K.; Suzuki, K.; Hirono, S. *J. Am. Chem. Soc.* **2006**, *128*, 7144–7145.
- (23) Morteza Najarian, A.; Szeto, B.; Tefashe, U. M.; McCreery, R. L. *ACS Nano* **2016**, *10*, 8918–8928.
- (24) Yan, H.; Bergren, A. J.; McCreery, R. L. *J. Am. Chem. Soc.* **2011**, *133*, 19168–19177.
- (25) Tefashe, U. M.; Nguyen, Q. V.; Lafolet, F.; Lacroix, J.-C.; McCreery, R. L. *J. Am. Chem. Soc.* **2017**, *139*, 7436–7439.
- (26) Ivashenko, O.; Bergren, A. J.; McCreery, R. L. *Adv. Electr. Mater.* **2016**, *2*, 1600351.
- (27) Ivashenko, O.; Bergren, A. J.; McCreery, R. L. *J. Am. Chem. Soc.* **2016**, *138*, 722–725.
- (28) Nioradze, N.; Chen, R.; Kim, J.; Shen, M.; Santhosh, P.; Amemiya, S. *Anal. Chem.* **2013**, *85*, 6198–6202.
- (29) Velicky, M.; Bissett, M. A.; Toth, P. S.; Patten, H. V.; Worrall, S. D.; Rodgers, A. N. J.; Hill, E. W.; Kinloch, I. A.; Novoselov, K. S.; Georgiou, T.; Britnell, L.; Dryfe, R. A. W. *Phys. Chem. Chem. Phys.* **2015**, *17*, 17844–17853.
- (30) Kim, J.; Shen, M.; Nioradze, N.; Amemiya, S. *Anal. Chem.* **2012**, *84*, 3489–3492.
- (31) Nioradze, N.; Kim, J.; Amemiya, S. *Anal. Chem.* **2011**, *83*, 828–835.
- (32) Kim, J.; Izadyar, A.; Nioradze, N.; Amemiya, S. *J. Am. Chem. Soc.* **2013**, *135*, 2321–2329.
- (33) Kim, J.; Renault, C.; Nioradze, N.; Arroyo-Currás, N.; Leonard, K. C.; Bard, A. J. *J. Am. Chem. Soc.* **2016**, *138*, 8560–8568.
- (34) Kim, J.; Kim, B.-K.; Cho, S. K.; Bard, A. J. *J. Am. Chem. Soc.* **2014**, *136*, 8173–8176.
- (35) Kim, J.; Bard, A. J. *J. Am. Chem. Soc.* **2016**, *138*, 975–979.
- (36) Kim, J.; Renault, C.; Nioradze, N.; Arroyo-Currás, N.; Leonard, K. C.; Bard, A. J. *Anal. Chem.* **2016**, *88*, 10284–10289.
- (37) Kuo, T.-C.; McCreery, R. L. *Anal. Chem.* **1999**, *71*, 1553–1560.
- (38) Ambrosi, A.; Bonanni, A.; Sofer, Z.; Pumera, M. *Nanoscale* **2013**, *5*, 2379–2387.
- (39) Ambrosi, A.; Chua, C. K.; Bonanni, A.; Pumera, M. *Chem. Rev.* **2014**, *114*, 7150–7188.
- (40) Brownson, D. A. C.; Banks, C. E. *Phys. Chem. Chem. Phys.* **2011**, *13*, 15825–15828.
- (41) DuVall, S.; McCreery, R. L. *J. Am. Chem. Soc.* **2000**, *122*, 6759–6764.
- (42) Allred, C.; McCreery, R. L. *Anal. Chem.* **1992**, *64*, 444.
- (43) Chen, P.; McCreery, R. L. *Anal. Chem.* **1996**, *68*, 3958–3965.
- (44) Chen, P.; Fryling, M.; McCreery, R. L. *Anal. Chem.* **1995**, *67*, 3115.
- (45) Tan, S. Y.; Lazenby, R. A.; Bano, K.; Zhang, J.; Bond, A. M.; Macpherson, J. V.; Unwin, P. R. *Phys. Chem. Chem. Phys.* **2017**, *19*, 8726–8734.
- (46) Snowden, M. E.; Güell, A. G.; Lai, S. C. S.; McKelvey, K.; Ebejer, N.; O'Connell, M. A.; Colburn, A. W.; Unwin, P. R. *Anal. Chem.* **2012**, *84*, 2483–2491.
- (47) Güell, A. G.; Ebejer, N.; Snowden, M. E.; Macpherson, J. V.; Unwin, P. R. *J. Am. Chem. Soc.* **2012**, *134*, 7258–7261.
- (48) Amemiya, S. *Anal. Chem.* **2017**, *89*, 7269–7272.
- (49) Tan, S. Y.; Zhang, J.; Bond, A. M.; Macpherson, J. V.; Unwin, P. R. *Anal. Chem.* **2017**, *89*, 7273–7276.
- (50) Tan, S.-Y.; Perry, D.; Unwin, P. R. *J. Electroanal. Chem.* [Online early access]. DOI: [10.1016/j.jelechem.2017.10.044](https://doi.org/10.1016/j.jelechem.2017.10.044). Published Online: Oct 24, 2017. <http://www.sciencedirect.com/science/article/pii/S1572665717307531> (accessed Nov. 1, 2017).
- (51) Lefrou, C. *J. Electroanal. Chem.* **2006**, *592*, 103–112.
- (52) Bard, A. J.; Faulkner, L. R. *Electrochemical Methods: Fundamentals and Applications*, 2nd ed.; John Wiley & Sons: New York, 2001; p 239.
- (53) Marcus, R. A. *J. Chem. Phys.* **1965**, *43*, 679–701.
- (54) Nielson, R. M.; McManis, G. E.; Weaver, M. J. *J. Phys. Chem.* **1989**, *93*, 4703–4706.
- (55) Hupp, J. T.; Liu, H. Y.; Farmer, J. K.; Gennett, T.; Weaver, M. J. *J. Electroanal. Chem. Interfacial Electrochem.* **1984**, *168*, 313–334.
- (56) Kneten, K.; McCreery, R. L. *Anal. Chem.* **1992**, *64*, 2518–2524.
- (57) Penner, R. M.; Heben, M. J.; Longin, T. L.; Lewis, N. S. *Science* **1990**, *250*, 1118–1121.
- (58) Velmurugan, J.; Sun, P.; Mirkin, M. V. *J. Phys. Chem. C* **2009**, *113*, 459–464.
- (59) Güell, A. G.; Meadows, K. E.; Dudin, P. V.; Ebejer, N.; Macpherson, J. V.; Unwin, P. R. *Nano Lett.* **2014**, *14*, 220–224.